







## Article

# Modification of MCM-22 Zeolite and Its Derivatives with Iron for the Application in N<sub>2</sub>O Decomposition

Małgorzata Rutkowska <sup>1,\*</sup>, Aleksandra Jankowska <sup>1</sup>, Ewelina Różycka-Dudek <sup>1</sup>,  
Wiktor Dubiel <sup>1</sup>, Andrzej Kowalczyk <sup>1</sup>, Zofia Piwowska <sup>1</sup>, Sebastián Llopis <sup>2</sup>,  
Urbano Díaz <sup>2</sup> and Lucjan Chmielarz <sup>1</sup>

<sup>1</sup> Faculty of Chemistry, Jagiellonian University, Gronostajowa 2, 30-387 Kraków, Poland; a.jankowska@doctoral.uj.edu.pl (A.J.); ewelinarozyczkaa@gmail.com (E.R.-D.); wiktoria.dubiel@student.uj.edu.pl (W.D.); kowalczy@chemia.uj.edu.pl (A.K.); piwowska@chemia.uj.edu.pl (Z.P.); lucjan.chmielarz@uj.edu.pl (L.C.)

<sup>2</sup> Instituto de Tecnología Química, Universitat Politècnica de València–Consejo Superior de Investigaciones Científicas, Avd. de los Naranjos s/n, 46022 Valencia, Spain; sellope@upvnet.upv.es (S.L.); udiaz@itq.upv.es (U.D.)

\* Correspondence: malgorzata.rutkowska@uj.edu.pl; Tel.: +48-12-686-2429

Received: 9 September 2020; Accepted: 30 September 2020; Published: 2 October 2020



**Abstract:** Layered 2D zeolite MCM-22 and its delaminated derivative, ITQ-2, were modified with iron, by different methods (ion-exchange and direct synthesis), and with the use of different precursors (FeSO<sub>4</sub>·7H<sub>2</sub>O, Fe(NO<sub>3</sub>)<sub>3</sub>·9H<sub>2</sub>O, and [Fe<sub>3</sub>(OCOCH<sub>3</sub>)<sub>7</sub>·OH·2H<sub>2</sub>O]NO<sub>3</sub> oligocations. The applied modifications were aimed at optimization of iron form in the samples (aggregation, amount, location, and reducibility), in order to achieve the highest catalytic activity in the N<sub>2</sub>O decomposition. The synthesis of the samples was verified with the use of XRD (X-Ray Diffraction), N<sub>2</sub>-sorption and ICP-OES (Inductively Coupled Plasma Optical Emission Spectroscopy) techniques, while the form of iron in the samples was investigated by UV-vis-DRS (UV-vis diffuse reflectance spectroscopy), H<sub>2</sub>-TPR (Hydrogen Temperature-Programmed Reduction) and HRTEM (High-Resolution Transmission Electron Microscopy). The highest activity in the N<sub>2</sub>O decomposition presented the sample Fe(O,IE)MCM-22, prepared by ion-exchange of MCM-22 with Fe<sup>3</sup>(III) oligocations. This activity was related to the oligomeric Fe<sub>x</sub>O<sub>y</sub> species (the main form of iron in the sample) and the higher loading of active species (in comparison to the modification with FeSO<sub>4</sub>·7H<sub>2</sub>O).

**Keywords:** iron aggregation; oligocations; MCM-22; ITQ-2; layered zeolites; N<sub>2</sub>O decomposition

## 1. Introduction

MCM-22 zeolite, synthesized in the 1990s, by the Mobil researches [1], due to its unusual pore structure, combining large 12 MR (Membered Ring) cavities and medium (10 MR channels) pores, as well as specific 2D alignment of the zeolitic layers, is under a great scientist's interest for possible application in catalysis. The up-to-date papers reporting catalytic activity of MCM-22 have shown its high efficiency in various reactions, including alkylation [2–5], aromatization [6,7], methanol-to-olefin (MTO) or -hydrocarbon (MTH) conversions [8,9], glycerol conversion [10,11], cracking reactions [12,13], Fischer–Tropsch synthesis [14], Knoevenagel condensation [15],  $\alpha$ -pinene isomerization [16,17], and in various environmental processes [18,19].

The specific 2D structure of MCM-22 enables its use as a lamellar precursor for preparation of other zeolitic materials, with increased accessibility of active sites (increased surface area and generated mesoporosity). Swollen parent MCM-22(P) material subjected to pillarization or exfoliation processes results in MCM-36 [20] (layers separated by pillars, face-to-face orientation) and in ITQ-2 [21]

(random orientation of layers, preferentially edge-to-face, so-called house-of-cards structure) materials. The relatively simple procedure used for the ITQ-2 synthesis results in material composed of sheets (2.5 nm thick), with the easy accessible 12 MR cups, whose entrances were not available for the catalyzed molecules in calcined 3D MCM-22 zeolite [22,23]. Such modification of the MCM-22 layers' alignment to form ITQ-2 was found to be very attractive for various catalytic processes. Osman et al. [2] investigated the catalytic activity of ITQ-2 with different delamination degree in alkylaromatic transformation and confirmed the positive effect of delamination, regarding the selectivity to alkylation product (alkylation was favored vs. disproportionation). Carriço et al. [10] found ITQ-2 to be more catalytically active than MCM-22 and MCM-36 in glycerol dehydration to acrolein and assigned this effect to the improved textural and acidic properties of this zeolitic material. Similarly, a positive effect of delamination was observed by Hao et al. [14], in Fischer–Tropsch reaction over Co-modified MCM-22 derivatives.

Nitrous oxide emission abatement is considered to be one of the current goals in environmental heterogeneous catalysis. The main  $\text{N}_2\text{O}$  emitter is chemical industry, specifically adipic acid, nitric acid, and nitrogen fertilizers' production plants [24]. Since nitrous oxide was identified as a strong greenhouse gas, contributing to the ozone layer's destruction [25], ongoing research on its catalytic conversion in flue gases has been carried out. Among different catalysts tested in this reaction Fe-modified zeolites (e.g., see References [26–29]), co-spinel-based materials (e.g., see References [30–34]), and mixed metal oxides (e.g., see References [35–38]) were found to be the most active and promising candidates for the large-scale application. High interest in iron modified zeolites is connected with their high activity, non-toxicity, and relatively simple and cheap modification procedures, as well as their relatively high insensitivity for other  $\text{N}_2\text{O}$  components of real waste gases, such as  $\text{O}_2$ ,  $\text{NO}$ ,  $\text{SO}_2$ , or  $\text{H}_2\text{O}$  [27].

Depending on the iron precursor, the method of its deposition, and the type of the support used, different forms of this metal can be formed in the catalyst. Starting from framework isomorphous substituted  $\text{Fe}^{3+}$ , through  $\text{Fe}^{3+}$  and  $\text{Fe}^{2+}$  monomeric cations (interacting with Si-O- and Al-O- bridges), di-nuclear Fe-O-Fe species, oligomeric oxo-species, and finally bulky  $\text{Fe}_x\text{O}_y$  particles can be formed [39]. In the case of  $\text{N}_2\text{O}$  decomposition, the majority of the scientific reports emphasize the high activity of the extra-framework iron sites (so-called  $\alpha$ -sites), which are able to form highly active surface oxygen. The active  $\alpha$ -sites are binuclear  $\text{Fe}^{2+}$  clusters (redox switch between  $\text{Fe}^{2+}$  and  $\text{Fe}^{3+}$ ) [40,41]. Pérez-Ramírez et al. [26,42] revealed high activity of oligonuclear Fe species, which are preferred over isolated  $\text{Fe}^{3+}$  cations, and found that framework iron and iron oxide particles are inactive in  $\text{N}_2\text{O}$  decomposition.

In the presented work, MCM-22 zeolite and its derivative, ITQ-2, were modified with iron, using different metal precursors— $\text{FeSO}_4 \cdot 7\text{H}_2\text{O}$  (S),  $\text{Fe}(\text{NO}_3)_3 \cdot 9\text{H}_2\text{O}$  (N), and  $[\text{Fe}_3(\text{OCOCH}_3)_7 \cdot \text{OH} \cdot 2\text{H}_2\text{O}]\text{NO}_3$  (O), as well as different methods of metal precursor deposition, i.e., ion-exchange (IE) or direct synthesis (DS). Different states, aggregations, and loadings of deposited iron species determined their catalytic activity in  $\text{N}_2\text{O}$  decomposition.

## 2. Results

### 2.1. MCM-22 and ITQ-2 Modified with $\text{FeSO}_4 \cdot 7\text{H}_2\text{O}$ and $[\text{Fe}_3(\text{OCOCH}_3)_7 \cdot \text{OH} \cdot 2\text{H}_2\text{O}]\text{NO}_3$ by Ion-Exchange

The zeolitic structure of the synthesized MCM-22 and ITQ-2 samples was confirmed by XRD measurements (Figure 1). The XRD pattern obtained for the parent MCM-22(P) sample is characteristic of MWW zeolites family and the presence of the (002) reflection at  $2\theta$  about  $6.5^\circ$  (d-spacing  $\sim 2.7$  nm) confirms the layers' separation and 2D structure of the as-synthesized material [43,44]. After calcination, the (002) reflection disappeared, indicating condensation of the zeolite layers (sample MCM-22). Other intra-layer reflections, like (100), remained unchanged or became sharper after template removal. In the case of delaminated material, both before (ITQ-2(P)) and after calcination (ITQ-2), the (002) reflection is absent. This phenomenon is connected with disordered structure of ITQ-2 formed under conditions of MCM-22(P) post-synthesis treatment with ultrasounds. However, it is worth noting that

this treatment did not destroy the structure of the MWW layers, and the intra-layer (100) reflection remained unchanged in the case of delaminated samples.

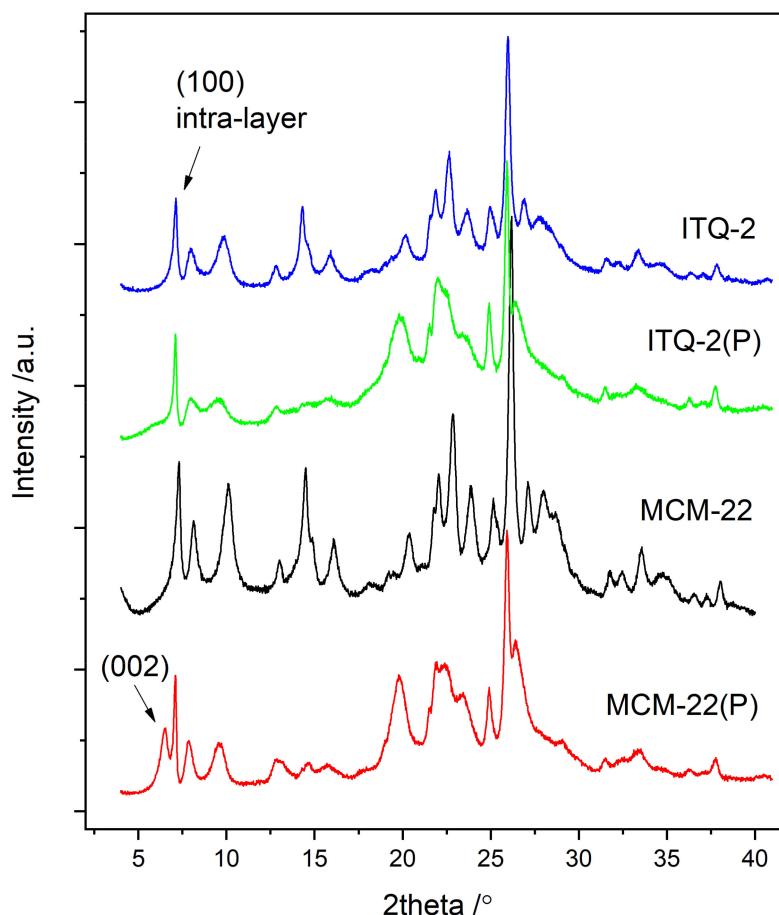


**Figure 1.** XRD patterns of MCM-22 and ITQ-2 zeolites before and after calcination.

Textural properties of the synthesized MCM-22 and ITQ-2 samples were determined by  $N_2$ -sorption (Table 1). The BET (Brunauer–Emmett–Teller) surface area and volume of micropores determined for delaminated ITQ-2 sample slightly decreased in comparison to MCM-22, which could be connected with the limitation of the ordered microporous structure to the separate layers in ITQ-2, in comparison to the three-dimensional microporous structure in MCM-22. These changes were accompanied by a significant increase in the external surface area and volume of mesopores, which proved the successful opening of the zeolite structure by generation of mesopores between the disordered MWW layers (so-called house-of-cards structure).

Both MCM-22 and ITQ-2 were modified with iron by ion-exchange (IE) using two types of iron precursors— $FeSO_4 \cdot 7H_2O$  (S) and  $[Fe_3(OCOCH_3)_7 \cdot OH \cdot 2H_2O]NO_3$  (O) oligocations (sample codes, modification methods and iron precursors are presented in Table 1). The amount and state (aggregation, location, reducibility) of iron species in the samples were investigated by ICP-OES, UV-vis-DRS, TEM, and  $H_2$ -TPR methods. The use of  $FeSO_4 \cdot 7H_2O$  as iron precursor resulted in introduction of about 1 wt% of iron into both MCM-22 and ITQ-2 (Table 1). The use of iron oligocations, despite the same method of zeolitic supports modification (ion-exchange), resulted in much higher iron loadings. Seems that in the case of  $Fe_3(III)$  oligocation solution, besides the ion-exchange, also precipitation of iron particles on the surface of zeolite grains or crystallites could occur, which resulted in increased iron loading.

**Table 1.** Textural parameters determined by N<sub>2</sub> sorption, iron content measured by ICP-OES, and H<sub>2</sub>/Fe ratio estimated based on H<sub>2</sub>-TPR.

Sample Code.	Iron Source	Modification Method	S <sub>BET</sub> /m <sup>2</sup> /g	S <sub>EXT</sub> /m <sup>2</sup> /g	V <sub>MIC</sub> /cm <sup>3</sup> /g	V <sub>MES</sub> /cm <sup>3</sup> /g	Fe (%)	H <sub>2</sub> /Fe
MCM-22	—	—	622	117	0.202	0.281	—	—
ITQ-2	—	—	608	186	0.178	0.384	—	—
Fe(S,IE)MCM-22	S	IE	611	117	0.198	0.287	0.82	1.44
Fe(S,IE)ITQ-2	S	IE	586	173	0.173	0.359	0.80	1.29
Fe(O,IE)MCM-22	O	IE	519	131	0.156	0.285	12.67	0.45
Fe(O,IE)ITQ-2	O	IE	519	173	0.145	0.353	9.79	0.43
Fe0.25(N,DS)MCM-22	N	DS	614	53	0.223	0.125	1.65	0.83
Fe1(N,DS)MCM-22	N	DS	514	69	0.177	0.171	3.40	0.56
Fe2(N,DS)MCM-22	N	DS	563	79	0.193	0.200	4.50	0.56
Fe4(N,DS)MCM-22	N	DS	531	74	0.183	0.177	5.28	0.43
Fe(N,DS)MCM-22	N	DS	561	74	0.195	0.178	6.51	0.51
Fe2(N/S,DS/IE)MCM-22	N/S	DS/IE	542	92	0.180	0.219	6.70	0.48
Fe2(N/O,DS/IE)MCM-22	N/O	DS/IE	473	100	0.149	0.217	13.50	0.43

S—FeSO<sub>4</sub>·7H<sub>2</sub>O; N—Fe(NO<sub>3</sub>)<sub>3</sub>·9H<sub>2</sub>O; O—[Fe<sub>3</sub>(OCOCH<sub>3</sub>)<sub>7</sub>·OH·2H<sub>2</sub>O]NO<sub>3</sub>; IE—ion-exchange; DS—direct synthesis; S<sub>BET</sub>—Brunauer–Emmett–Teller (BET) surface area; S<sub>EXT</sub>—external surface area; V<sub>MIC</sub>—volume of micropores; V<sub>MES</sub>—volume of mesopores.

The form of introduced iron species in the samples was investigated by UV–vis-DR spectroscopy. The sub-bands, distinguished in Figure 2 by deconvolution of the original spectra, are assigned to monomeric Fe<sup>3+</sup> cations (absorption below 300 nm), oligomeric Fe<sub>x</sub>O<sub>y</sub> species (absorption at about 300–400 nm) and small iron oxide crystallites (absorption at above 400 nm) [45]. Significant differences in the UV–vis spectra of the samples modified with different iron precursors were observed. The Fe(S,IE)MCM-22 and Fe(S,IE)ITQ-2 samples obtained by ion-exchange method with FeSO<sub>4</sub>·7H<sub>2</sub>O solution contain iron in the less aggregated forms, mainly monomeric cations, both in tetrahedral and octahedral coordination, indicated by maxima at about 225 and 275 nm, respectively. Moreover, small contribution of oligomeric Fe<sub>x</sub>O<sub>y</sub> species in these samples was identified by absorption at about 350 nm. In the case of the Fe(O,IE)MCM-22 and Fe(O,IE)ITQ-2 samples modified with Fe<sub>3</sub>(III) oligocations, according to our expectations, iron was introduced in more aggregated forms. The contribution of oligomeric iron oxide species in these samples is more significant, which confirms successful deposition of iron oligocations. Moreover, in the spectra of Fe(O,IE)MCM-22 and Fe(O,IE)ITQ-2, the absorption bands characteristic of bulky iron oxide species are present, indicating possible sintering of iron oligomeric species under calcination conditions. A comparison of MCM-22 and ITQ-2 supports showed higher aggregation of iron species in former microporous zeolite. Mesoporosity generated in ITQ-2 and its open porous structure favored deposition of iron in the form of monomeric cations and small oligomeric iron oxide species instead of more aggregated ones.

The morphology of the MCM-22 and ITQ-2 samples modified with FeSO<sub>4</sub>·7H<sub>2</sub>O and [Fe<sub>3</sub>(OCOCH<sub>3</sub>)<sub>7</sub>·OH·2H<sub>2</sub>O]NO<sub>3</sub> by the ion-exchange method was analyzed by HRTEM microscopy (Figure 3). For the samples modified with FeSO<sub>4</sub>·7H<sub>2</sub>O (Figure 3a,b), only the arrangement of zeolite MWW layers was visible and any agglomerated iron species were found. It is worth noting that the topology of the Fe-ITQ-2 sample presents a looser arrangement of layers than in the case of Fe-MCM-22, which was expected after the delamination process. For the samples modified with Fe<sub>3</sub>(III) oligocations (Figure 3c,d), distinct bulky iron aggregates, with the size of about 5 nm, were found. Both the Fe(O,IE)MCM-22 and Fe(O,IE)ITQ-2 samples are characterized by uniform distribution of iron oxide particles on the surface. The analysis of the samples by HRTEM microscopy is consistent with the type of iron species identified in the samples by UV–vis-DR spectroscopy.

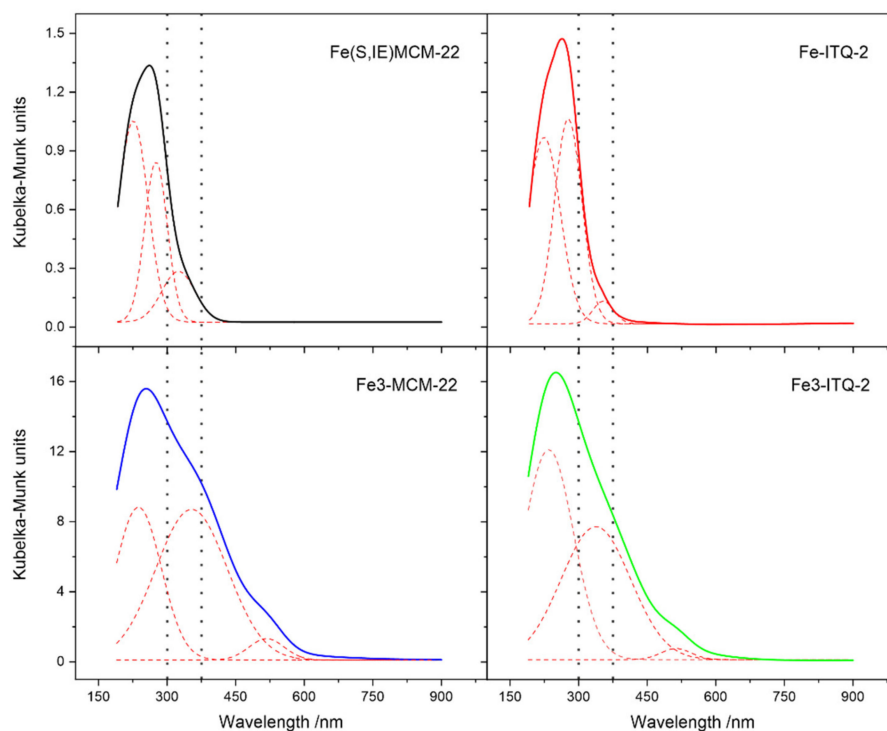


**Figure 2.** UV-vis-DR spectra of the MCM-22 and ITQ-2 samples modified with  $\text{FeSO}_4 \cdot 7\text{H}_2\text{O}$  and  $[\text{Fe}_3(\text{OCOCH}_3)_7 \cdot \text{OH} \cdot 2\text{H}_2\text{O}]\text{NO}_3$  by ion-exchange method.

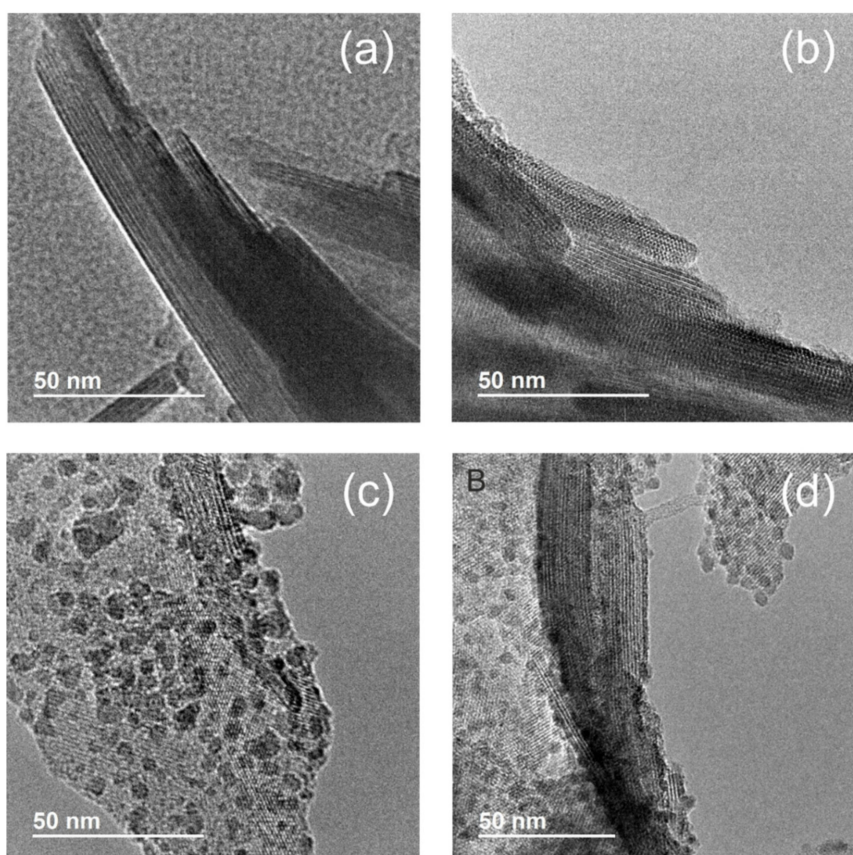


**Figure 3.** HRTEM micrographs of the MCM-22 and ITQ-2 samples modified with  $\text{FeSO}_4 \cdot 7\text{H}_2\text{O}$  and  $[\text{Fe}_3(\text{OCOCH}_3)_7 \cdot \text{OH} \cdot 2\text{H}_2\text{O}]\text{NO}_3$  by ion-exchange: (a)  $\text{Fe}(\text{S,IE})\text{MCM-22}$ , (b)  $\text{Fe}(\text{S,IE})\text{ITQ-2}$ , (c)  $\text{Fe}(\text{O,IE})\text{MCM-22}$ , and (d)  $\text{Fe}(\text{O,IE})\text{ITQ-2}$ .

Red-ox properties of the MCM-22 and ITQ-2 samples modified with  $\text{FeSO}_4 \cdot 7\text{H}_2\text{O}$  and  $[\text{Fe}_3(\text{OCOCH}_3)_7 \cdot \text{OH} \cdot 2\text{H}_2\text{O}]\text{NO}_3$  oligocations by ion-exchange method were analyzed by using the  $\text{H}_2$ -TPR method (Figure 4). The main  $\text{H}_2$  consumption peak present in the reduction profiles of all the samples, at about  $420^\circ\text{C}$ , can be assigned to the reduction of monomeric iron cations  $\text{Fe}^{3+} \rightarrow \text{Fe}^{2+}$  in ion-exchange positions [46]. This maximum dominated in the reduction profiles of the samples modified with  $\text{FeSO}_4 \cdot 7\text{H}_2\text{O}$  solution (Fe-MCM-22 and Fe-ITQ-2), but also small shoulders at about  $550^\circ\text{C}$  and above  $700^\circ\text{C}$  were found. They could be assigned to the reduction of  $\text{Fe}^{3+}$  cations in oligomeric species to  $\text{Fe}^{2+}$  and then reduction of  $\text{Fe}^{2+} \rightarrow \text{Fe}^0$ , respectively [46,47]. In the profiles of the samples modified with  $\text{Fe}_3(\text{III})$  oligocations (Fe(O,IE)MCM-22 and Fe(O,IE)ITQ-2), three distinct  $\text{H}_2$  consumption peaks were observed. Despite the reduction of monomeric  $\text{Fe}^{3+}$  cations at about  $420^\circ\text{C}$ , the reduction of larger iron oxide agglomerates and oligomeric species (below  $300^\circ\text{C}$  and about  $550^\circ\text{C}$ , respectively) were found [46,47]. It is worth noting that the reduction of the samples modified with  $\text{Fe}_3(\text{III})$  oligocations started at lower temperatures (about  $130^\circ\text{C}$ ) than in the case of the samples modified with monomeric  $\text{Fe}(\text{II})$  cations (about  $220^\circ\text{C}$ ). The results of the  $\text{H}_2$ -TPR measurements are fully consistent with UV-vis-DRS analysis (Figure 2), with respect to the identified types of iron species.

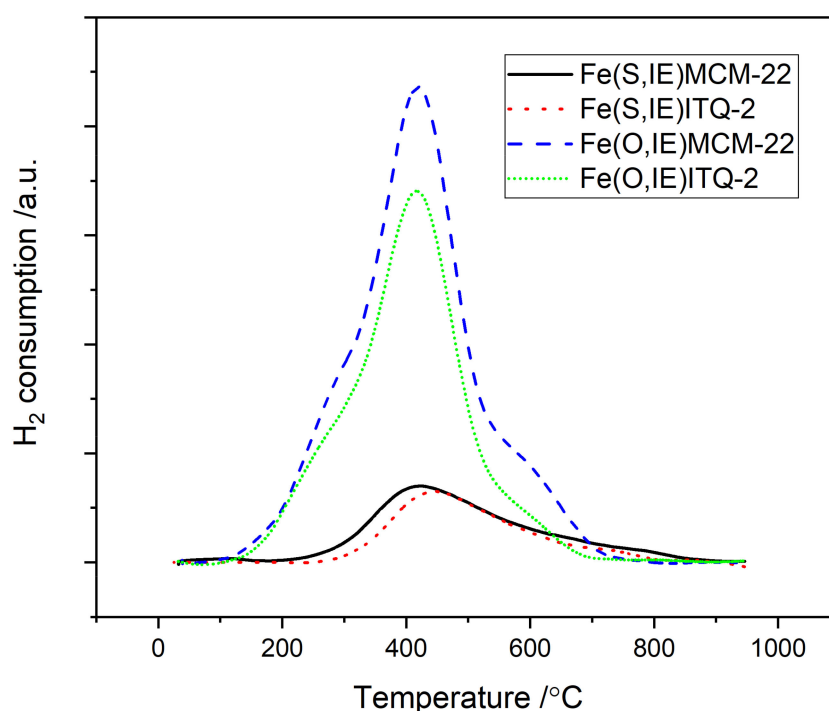


**Figure 4.**  $\text{H}_2$ -TPR profiles of the MCM-22 and ITQ-2 samples modified with  $\text{FeSO}_4 \cdot 7\text{H}_2\text{O}$  and  $[\text{Fe}_3(\text{OCOCH}_3)_7 \cdot \text{OH} \cdot 2\text{H}_2\text{O}]\text{NO}_3$  by ion-exchange.

Based on the total consumption of  $\text{H}_2$  from the  $\text{H}_2$ -TPR measurements and iron content in the samples measured by the ICP-OES method, the molar  $\text{H}_2/\text{Fe}$  ratio was calculated (Table 1). Complete reduction of  $\text{Fe}^{3+}$  in different iron species to  $\text{Fe}^0$  ( $\text{Fe}_2\text{O}_3 + 3\text{H}_2 \rightarrow 2\text{Fe}^0 + 3\text{H}_2\text{O}$ ) needs the hydrogen consumption equal to the  $\text{H}_2/\text{Fe}$  ratio of 1.5, while the reduction of  $\text{Fe}^{3+}$  to  $\text{Fe}^{2+}$  ( $\text{Fe}_2\text{O}_3 + \text{H}_2 \rightarrow 2\text{FeO} + \text{H}_2\text{O}$ ) hydrogen consumption equal to the  $\text{H}_2/\text{Fe}$  ratio of 0.5. Thus, the analysis of the  $\text{H}_2/\text{Fe}$  ratio could give information about the reduction level of the samples. In the case of the samples modified with  $\text{FeSO}_4 \cdot 7\text{H}_2\text{O}$ , the  $\text{H}_2/\text{Fe}$  ratio is close to 1.5, indicating almost complete reduction of iron species into  $\text{Fe}^0$  (broad  $\text{H}_2$  reduction at about  $700\text{--}800^\circ\text{C}$ , Figure 4). Similar results were reported by Romero-Sáez et al. [47], in the case of iron modified ZSM-5, with iron loadings of about 1.8 wt%. On the other side, for the samples modified with  $\text{Fe}_3(\text{III})$  oligocations (Fe(O,IE)MCM-22 and Fe(O,IE)ITQ-2), the  $\text{H}_2/\text{Fe}$  ratio is close to 0.5, indicating reduction of iron species to  $\text{Fe}^{2+}$ . The differences in reduction level observed between the samples modified with  $\text{FeSO}_4 \cdot 7\text{H}_2\text{O}$  and  $[\text{Fe}_3(\text{OCOCH}_3)_7 \cdot \text{OH} \cdot 2\text{H}_2\text{O}]\text{NO}_3$

oligocations could be connected with the form and amount of introduced Fe. Based on the obtained results, it was found that highly dispersed iron (low metal loadings) was more easily reduced to  $\text{Fe}^0$  than iron in the more aggregated forms. In the case of the samples modified with  $\text{Fe}_3(\text{III})$  oligocations, the reduction  $\text{Fe}^{2+} \rightarrow \text{Fe}^0$  possibly needs higher temperatures (e.g., see Reference [46], zeolites modified with 5 wt% of iron by wet impregnation). It should be noted that the obtained  $\text{H}_2/\text{Fe}$  ratios are only estimations and represent the average oxidation states of iron in various species.

Modification of the samples with iron, both with monomeric (S) and oligomeric (O) species, resulted in a slight decrease of their porosity (Table 1). This effect is more distinct for the  $\text{Fe}(\text{O,IE})\text{MCM-22}$  and  $\text{Fe}(\text{O,IE})\text{ITQ-2}$  samples (micropore volume decreased from  $0.202 \text{ cm}^3/\text{g}$  and  $0.178 \text{ cm}^3/\text{g}$  to  $0.156 \text{ cm}^3/\text{g}$  and  $0.145 \text{ cm}^3/\text{g}$ , respectively), which could be connected with the blocking of micropores by iron oxide aggregates or deposition of highly dispersed iron species inside the pores.

The catalytic activity of the MCM-22 and ITQ-2 samples modified with  $\text{FeSO}_4 \cdot 7\text{H}_2\text{O}$  and  $[\text{Fe}_3(\text{OCOCH}_3)_7 \cdot \text{OH} \cdot 2\text{H}_2\text{O}]\text{NO}_3$  by the ion-exchange method in the reaction of  $\text{N}_2\text{O}$  decomposition is presented in Figure 5. All the examined samples were catalytically active in the  $\text{N}_2\text{O}$  decomposition (Figure 5a). However, the comparison of the samples modified with different iron precursors showed higher catalytic activity of the samples modified with  $\text{Fe}_3(\text{III})$ . Moreover, MCM-22 used as catalytic support was found to be more active than ITQ-2. The observed differences can be connected with the loading of iron oligocations (ion-exchange with  $\text{Fe}_3(\text{III})$ ), which, under calcination conditions, formed catalytically active oligomeric  $\text{Fe}_x\text{O}_y$  species.

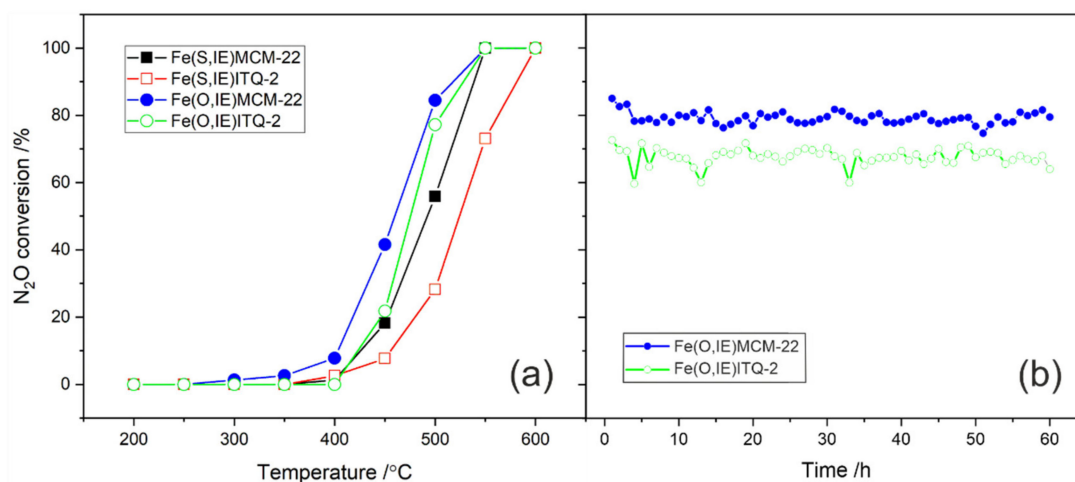


**Figure 5.**  $\text{N}_2\text{O}$  conversion (a) versus temperature for the MCM-22 and ITQ-2 samples modified with  $\text{FeSO}_4 \cdot 7\text{H}_2\text{O}$  and  $[\text{Fe}_3(\text{OCOCH}_3)_7 \cdot \text{OH} \cdot 2\text{H}_2\text{O}]\text{NO}_3$  by ion-exchange and (b) versus time for the samples  $\text{Fe}(\text{O,IE})\text{MCM-22}$  and  $\text{Fe}(\text{O,IE})\text{ITQ-2}$  at  $500^{\circ}\text{C}$ .

The most active catalysts,  $\text{Fe}(\text{O,IE})\text{MCM-22}$  and  $\text{Fe}(\text{O,IE})\text{ITQ-2}$ , were examined in isothermal stability tests at  $500^{\circ}\text{C}$  for 60 h (Figure 5b). For both catalysts the  $\text{N}_2\text{O}$  conversion slightly decreased during the first few hours of the test and then remained practically stable. Thus, it could be assumed that both types of zeolitic supports, as well as deposited iron species, introduced with the use of  $\text{Fe}_3(\text{III})$  precursor, were stable under conditions of the catalytic test.

Since any significant changes in the samples activity after delamination process of MCM-22 were observed, in the next step of the studies, conventional MCM-22 zeolite was chosen for further modifications (deposition of iron species by different methods and with the use of different iron precursors).

## 2.2. MCM-22 Zeolite Modified with $\text{Fe}(\text{NO}_3)_3 \cdot 9\text{H}_2\text{O}$ by Direct Synthesis

The samples of the  $\text{FeX}(\text{N,DS})\text{MCM-22}$  series (where X is the Fe/Al ratio, equal to 0.25, 1, 2, 4, and  $\infty$ ), were modified with iron by direct synthesis (DS), with the use of  $\text{Fe}(\text{NO}_3)_3 \cdot 9\text{H}_2\text{O}$  (N) (codes of the

samples are presented in Table 1). The structure of the samples was examined by XRD (Figure 6a), and in diffractograms recorded for all the samples, the characteristic fingerprint of MWW zeolite topology was identified. Independently from the iron content in the sample, similar XRD patterns were obtained, proving the successful synthesis of MCM-22 zeolites.

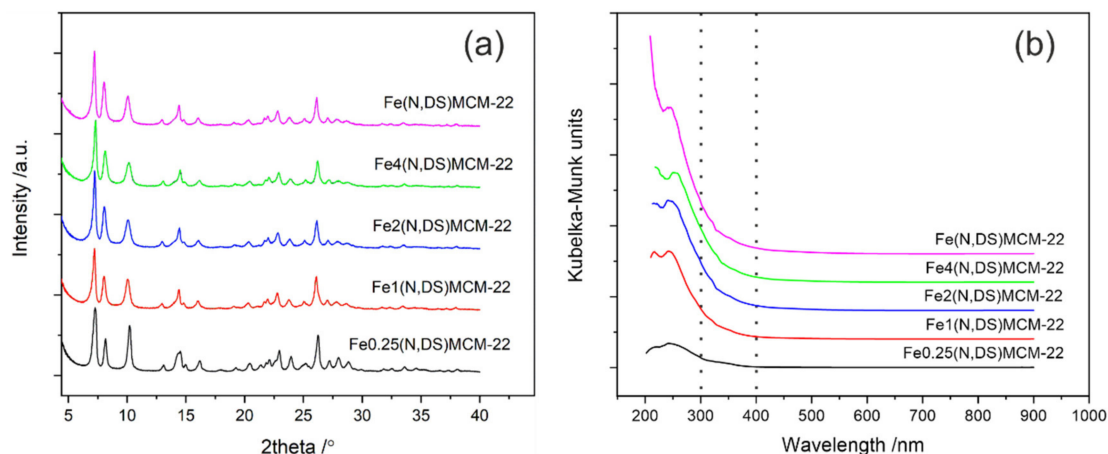


**Figure 6.** (a) XRD patterns and (b) UV-vis-DR spectra of the samples from FeX(N,DS)MCM-22 series, modified with iron by direct synthesis.

Textural parameters of the samples (Table 1) modified with iron by direct synthesis differ slightly depending on the content of introduced metal. However, a clear dependency was not observed. The most significant difference was found between the Fe0.25(N,DS)MCM-22 sample and other samples of this series, mainly connected with the microporous characteristic of zeolites. It seems that the introduction of a higher amount of iron into the zeolite framework decreased the volume of micropores and increased the external surface area and volume of mesopores of the samples. It is worth noting that this disorder of microporous structure observed for the Fe1(N,DS)MCM-22, Fe2(N,DS)MCM-22, Fe4(N,DS)MCM-22, and Fe(N,DS)MCM-22 samples was slight, and the zeolitic microporous character of the samples was maintained, even for the sample fully substituted with iron (without framework Al).

The percentage content of iron introduced into the samples, measured by using the ICP-OES method (Table 1), increased with the increasing molar Fe/Al (X) ratio in the FeX(N,DS)MCM-22 series. The intended Fe/Al ratios, assumed during the synthesis as 0.25, 1, 2, and 4, were calculated based on the results of the chemical analysis and were equal to 0.23, 0.9, 1.8, and 3.6, respectively. Thus, the real Fe/Al ratios are very close to the assumed ones, indicating the successful synthesis of the samples (slightly lower values of built-in framework metal are common in the case of zeolite synthesis [48]).

The form of iron (aggregation, coordination, and location) introduced into the samples of FeX(N,DS)MCM-22 series was investigated by UV-vis-DR spectroscopy (Figure 6b). For all the samples, absorption was observed mainly below 300 nm, which is connected with the presence of monomeric Fe<sup>3+</sup> cations in tetrahedral and octahedral coordination, indicated by maxima at about 215 and 250 nm, respectively [45]. This result is consistent with the used modification method, which assumed the introduction of iron into the zeolite framework. The results obtained by UV-vis-DR spectroscopy cannot strictly prove the successful incorporation of iron into the zeolite framework. However, it is important to note that about 6.5% of Fe was introduced by this method to the Fe(N,DS)MCM-22 sample (Table 1), and any significant aggregation of iron was observed. While, in the case of the samples modified by ion-exchange method (Fe(S,IE)MCM-22 and Fe(S,IE)ITQ-2, Table 1), aggregated Fe<sub>x</sub>O<sub>y</sub> oligomeric species were identified in the samples containing iron content as low as 1 wt% (Figure 2). Thus, it could be supposed that, to a significant extent, iron was introduced into the zeolite framework or, in some part, could be highly distributed among the ion-exchange positions, which prevented the sintering and agglomeration of iron particles. Slight absorption shoulder observed above 300 nm was rather connected with the absorption band centered at a lower wavelength than

with the presence of oligomeric species, but some negligible fraction of this iron form in the samples cannot be excluded.

The results of N<sub>2</sub>O decomposition performed over the samples of the FeX(N,DS)MCM-22 series, modified with iron by direct synthesis, are presented in Figure 7a. Catalytic activity of all the samples was similar and the N<sub>2</sub>O conversion over this series barely reached 100% at 600 °C. The highest conversion of N<sub>2</sub>O was obtained over the Fe<sub>0.25</sub>(N,DS)MCM-22 sample, which could be connected with its textural properties (larger BET surface area and micropore volume) rather than with iron loading. This conclusion resulted from the similar activity of other samples of this series, independently of iron content.

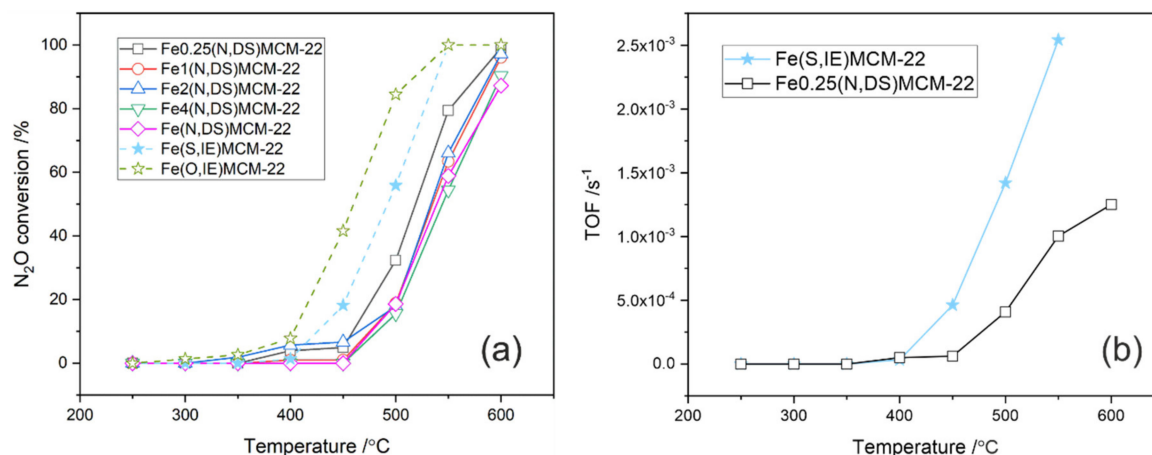


**Figure 7.** (a) Temperature dependence of N<sub>2</sub>O conversion over the samples from FeX(N,DS)MCM-22 series (modified with iron by direct synthesis), compared with the samples Fe(S,IE)MCM-22 and Fe(O,IE)MCM-22 (modified with iron by ion-exchange). (b) Temperature dependence of reaction rate for Fe(S,IE)MCM-22 and Fe<sub>0.25</sub>(N,DS)MCM-22.

Our comparison of the catalytic activity of these samples with Fe(S,IE)MCM-22 and Fe(O,IE)MCM-22 (profiles added to Figure 7a), modified by ion-exchange method, leads to the conclusion concerning the relationship between the form of iron species in the samples and their activity in N<sub>2</sub>O decomposition. The loading of iron in the series FeX(N,DS)MCM-22 is higher than in the case of the samples Fe(S,IE)MCM-22 and Fe(O,IE)MCM-22; however, they do not show higher catalytic activity. Thus, the catalytic efficiency of the samples in N<sub>2</sub>O decomposition should be related to the form of the introduced iron species. Iron in the form of monomeric Fe<sup>3+</sup> cations, present as a main iron form in the samples of the FeX(N,DS)MCM-22 series, showed significantly lower activity than more aggregated Fe<sub>x</sub>O<sub>y</sub> species present in Fe(S,IE)MCM-22 and Fe(O,IE)MCM-22. This difference in activity could be presented by means of turnover frequency (TOF), compared for two samples, namely Fe(S,IE)MCM-22 and Fe<sub>0.25</sub>(N,DS)MCM-22, modified by the ion-exchange method and by direct synthesis, respectively (Figure 7b). TOF, defined as a number of N<sub>2</sub>O molecules decomposed over one active site during 1 s of reaction, was calculated based on the measured N<sub>2</sub>O conversion (X), using Equation (1). Calculations were performed with the assumption that all iron cations present in the sample act as active sites.

$$TOF = \frac{\dot{n}_{N_2O}}{n_{Fe}} \cdot X \quad (1)$$

where  $\dot{n}_{N_2O}$  is molar flow of N<sub>2</sub>O (mol/s),  $n_{Fe}$  is total number of Fe moles measured by ICP (mol), and X is N<sub>2</sub>O conversion from the catalytic test (-).

Turnover frequency (Figure 7b), independently of the iron content in the samples, is much higher in the case of active sites in the more aggregated form (oligomeric Fe<sub>x</sub>O<sub>y</sub>), generated in Fe(S,IE)MCM-22 by ion exchange. Such results were previously observed for other zeolite topologies used as catalyst support (e.g., see References [26,42]).

Since better catalytic activity in  $N_2O$  decomposition was observed over the samples modified with iron by ion-exchange method, in the next step of the studies,  $Fe_2(N,DS)MCM-22$  was modified by the ion-exchange method (with different iron precursors) as the post-synthesis treatment.

### 2.3. $Fe_2(N,DS)MCM-22$ Zeolite Modified with Different Iron Precursors by Post-Synthesis Ion-Exchange

Modification of  $Fe_2(N,DS)MCM-22$  by ion-exchange method (IE) with  $FeSO_4 \cdot 7H_2O$  (S) (sample  $Fe_2(N/S,DS/IE)MCM-22$ ), and with  $[Fe_3(OCOCH_3)_7 \cdot OH \cdot 2H_2O]NO_3$  oligocations (O) (sample  $Fe_2(N/O,DS/IE)MCM-22$ ) slightly influenced textural parameters of the samples (Table 1). Introduction of additional metal species resulted in a decrease of BET surface area and micropore volume. These changes in textural parameters ( $S_{BET}$ ,  $V_{MIC}$ :  $Fe_2(N/S,DS/IE)MCM-22 > Fe_2(N/O,DS/IE)MCM-22$ ) could be connected with the increasing size of iron agglomerates, depending on the iron precursor used and blockage of the zeolite pores. On the other side, after subsequent modification of  $Fe_2(N,DS)MCM-22$  by ion-exchange method, the external surface area of the samples increased ( $S_{EXT}$ :  $Fe_2(N/S,DS/IE)MCM-22 < Fe_2(N/O,DS/IE)MCM-22$ ), which could be connected with the generation of additional porosity between the metal aggregates deposited on the sample surface.

The iron content in the samples, measured by using the ICP-OES method (Table 1), was much higher for  $Fe_2(N/O,DS/IE)MCM-22$ , modified with  $Fe_3(III)$  oligocations (13.5 wt%), while, for  $Fe_2(N/S,DS/IE)MCM-22$ , it was equal to 6.7 wt%. A similar tendency was observed for the  $Fe(S,IE)MCM-22$  and  $Fe(O,IE)MCM-22$  samples. It is worth mentioning that the content of iron in the samples obtained by double modification with iron (by direct synthesis and by post-synthesis ion-exchange) was higher than for the samples modified exclusively by the ion-exchange method.

The form of iron in the samples obtained by double modification (direct synthesis and post-synthesis ion-exchange method) was analyzed by UV-vis-DR spectroscopy (Figure 8a) and  $H_2$ -TPR (Figure 8b). In the case of both characterization methods, the results were compared with the results obtained for the  $Fe_2(N,DS)MCM-22$  sample (profiles added into the graphs). Our analysis of the UV-vis-DR spectra (Figure 8a) shows that subsequent modification with Fe by the ion-exchange method resulted in more aggregated iron species in comparison to  $Fe_2(N,DS)MCM-22$ . In the spectra of  $Fe_2(N/S,DS/IE)MCM-22$  and  $Fe_2(N/O,DS/IE)MCM-22$   $Fe_xO_y$  oligomers (absorption 300–400 nm), bulky iron oxide particles (absorption  $> 400$  nm) were identified [45]. The agglomeration effect was stronger in the case of post-synthesis ion-exchange with  $Fe_3(III)$  (O) oligocations than with a solution of monomeric  $Fe(II)$  (S). A similar relation was found between the  $Fe(S,IE)MCM-22$  and  $Fe(O,IE)MCM-22$  samples modified exclusively by ion-exchange. Similar observations could be made based on the TPR results (Figure 8b). In the obtained  $H_2$  consumption profiles, the reduction peaks related to highly agglomerated iron forms ( $< 300$  °C), reduction of monomeric  $Fe^{3+}$  cations (about 400 °C), and reduction oligomeric  $Fe_xO_y$  species (about 600 °C) could be distinguished [46,47]. For the samples doubly modified with iron, ( $Fe_2(N/S,DS/IE)MCM-22$  and  $Fe_2(N/O,DS/IE)MCM-22$ ), the  $H_2$  consumption connected with the reduction of agglomerated Fe forms was higher, which was more significant in the case of the samples ion-exchanged with  $Fe_3(III)$  oligocations. The analysis of the  $H_2/Fe$  ratio of the samples of this series (Table 1) suggested the reduction to  $Fe^{2+}$  (the  $H_2/Fe$  ratio about 0.5), similarly to the samples with high metal loading, prepared by ion-exchange with  $Fe_3(III)$  oligocations.

The results of  $N_2O$  decomposition over the catalysts doubly modified with iron are presented in Figure 9 (for comparison, the profiles of the  $Fe_2(N,DS)MCM-22$ ,  $Fe(S,IE)MCM-22$ , and  $Fe(O,IE)MCM-22$  samples were added).

$N_2O$  conversion over  $Fe(S,IE)MCM-22$  and  $Fe(O,IE)MCM-22$  was similar and reached only about 70% at 600 °C. Post-synthesis modification of  $Fe_2(N,DS)MCM-22$  by ion-exchange method did not increase the catalytic activity of the samples. The samples doubly modified with iron were characterized by significantly high iron loadings (Table 1) and by the presence of  $Fe_xO_y$  iron species (Figure 8). However, the synergetic effect of these factors (recognized earlier as connected with the high catalytic activity) was not found. The observed drop in the catalytic activity could be connected with the

overloading of the samples and blockage of the MCM-22 porous system by sintering of metal particles present on the surface.

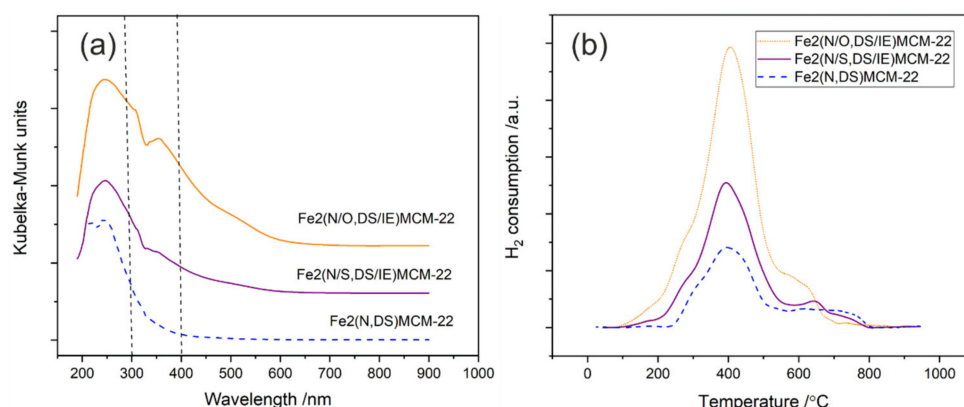


**Figure 8.** (a) UV-vis-DR spectra and (b) H<sub>2</sub>-TPR profiles of the samples Fe<sub>2</sub>(N,DS)MCM-22, Fe<sub>2</sub>(N/S,DS/IE)MCM-22, and Fe<sub>2</sub>(N/O,DS/IE)MCM-22.

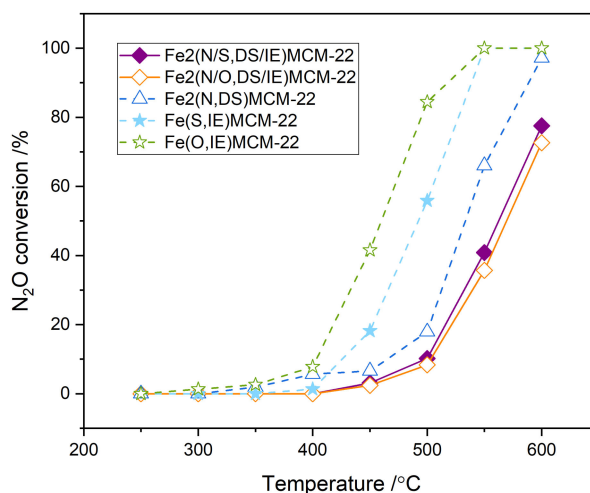


**Figure 9.** Temperature dependence of N<sub>2</sub>O conversion over the samples doubly modified with iron, compared with the Fe<sub>2</sub>(N,DS)MCM-22, Fe(S,IE)MCM-22, and Fe(O,IE)MCM-22 samples.

### 3. Materials and Methods

#### 3.1. Catalysts Synthesis

##### 3.1.1. MCM-22 and ITQ-2

The synthesis of MCM-22 (Si/Al = 15), described previously in detail in [18], proceeded in a basic solution of NaOH (POCH, Gliwice, Poland) with the use of hexamethyleneimine (99%, Aldrich, St. Louis, MO, USA) as structure directing agent, fumed silica (Aerosil 200, Overlack, Hanau, Germany) as silica source and NaAl<sub>2</sub>O<sub>3</sub> (Sigma-Aldrich, St. Louis, MO, USA) as alumina source. The obtained synthesis gel was mixed at ambient temperature for 2 h and aged in PTFE-lined stainless-steel autoclave with rotation (60 rpm) at 150 °C for 7 days. The obtained white solid parent MCM-22(P) was recovered by filtration and washed with distilled water. In the next step, the sample was dried at 60 °C and calcined at 600 °C, for 6 h, resulting in microporous 3-dimensional MCM-22.

ITQ-2 was prepared, starting from MCM-22(P), which was subjected to swelling procedure with the use of hexadecyltrimethylammonium bromide (Sigma-Aldrich, St. Louis, MO, USA) (~50% ion exchanged Br<sup>−</sup>/OH<sup>−</sup>, ~25 wt%) and tetrapropylammonium bromide (Sigma-Aldrich, St. Louis, MO, USA) (~50% ion exchanged Br<sup>−</sup>/OH<sup>−</sup>, ~40 wt %). Details of this procedure were previously presented in

Reference [18]. The swollen sample (MCM-22(S)) was sonicated in an ultrasound bath for 1 h, acidified to pH ~2 with concentrated HCl (POCH, Gliwice, Poland), centrifuged, and washed with distilled water. In a next step, the sample (ITQ-2(P)) was dried at 60 °C and calcined at 600 °C, for 6 h, resulting in ITQ-2.

Obtained MCM-22 and ITQ-2 materials were modified by ion exchange with  $\text{FeSO}_4 \cdot 7\text{H}_2\text{O}$  and  $[\text{Fe}_3(\text{OCOCH}_3)_7 \cdot \text{OH} \cdot 2\text{H}_2\text{O}]\text{NO}_3$  oligocations, according to the procedure described below. The sample codes are presented in Table 1.

### 3.1.2. FeX(N,DS)MCM-22 Modified with Fe(III) by Direct Synthesis

A series of FeX(N,DS)MCM-22, modified with iron by direct synthesis (DS), was prepared according to the recipe described in Reference [49]. The synthesis started from the preparation of two solutions: (1) sodium hydroxide (POCH, Gliwice, Poland) and aluminum hydroxide (Chempur, Piekary Śląskie, Poland) in  $\text{H}_2\text{O}$  and (2)  $\text{Fe}(\text{NO}_3)_3 \cdot 9\text{H}_2\text{O}$  (N) (Sigma-Aldrich, St. Louis, MO, USA) in  $\text{H}_2\text{O}$ . In the next step, Solution (2) was added dropwise to Solution (1), under stirring. To the resulting mixture, hexamethylenimine (99%, Aldrich, St. Louis, MO, USA) and fumed silica (Aerosil 200, Overlack, Hanau, Germany) were added, and the obtained slurry was stirred at ambient temperature for 2 h. In the next step, the synthesis gel was aged in PTFE-lined stainless-steel autoclave with rotation (60 rpm), at 150 °C, for 5 days. After the aging time, the samples were recovered by filtration, washed with distilled water, dried at 60 °C, and calcined at 600 °C for 6 h. In each synthesis, 7.2 g of fumed  $\text{SiO}_2$  was used, keeping the following formula:  $6\text{Na}_2\text{O} : 30\text{SiO}_2 : a\text{Al}_2\text{O}_3 : b\text{Fe}(\text{NO}_3)_3 : 1411\text{H}_2\text{O}$ , where *a* and *b* were adjusted to the Fe/Al ratio (X), which was assumed in the synthesis as 0.25, 1, 2, and 4 (for the comparison, the sample only with iron (without Al) was prepared, Fe(N,DS)MCM-22). For all the samples, the intended Si/Fe+Al ratio was 15.

The Fe2(N,DS)MCM-22 sample was additionally modified by the ion-exchange method with  $\text{FeSO}_4 \cdot 7\text{H}_2\text{O}$  and  $[\text{Fe}_3(\text{OCOCH}_3)_7 \cdot \text{OH} \cdot 2\text{H}_2\text{O}]\text{NO}_3$  oligocations, according to the procedure described below. The sample codes are presented in Table 1.

### 3.1.3. Ion-Exchange

Deposition of iron by the ion-exchange (IE) method was conducted with the use of the previously calcined and dried samples (overnight, at 110 °C). The samples were modified with aqueous solution of  $\text{FeSO}_4 \cdot 7\text{H}_2\text{O}$  (S) (Sigma-Aldrich, St. Louis, USA) or  $[\text{Fe}_3(\text{OCOCH}_3)_7 \cdot \text{OH} \cdot 2\text{H}_2\text{O}]\text{NO}_3$  oligocations (O).  $\text{Fe}_3(\text{III})$  oligocations were prepared according to References [50,51]. The synthesis started with dissolution of  $\text{Fe}(\text{NO}_3)_3 \cdot 9\text{H}_2\text{O}$  (Sigma-Aldrich, St. Louis, MO, USA) in anhydrous ethyl alcohol (99.8%, POCH, Gliwice, Poland). In a next step, acetic anhydride (> 98%, VWR, Leuven, Belgium) was added, dropwise, into this solution, under continuous stirring. The obtained mixture was cooled down (addition of acetic anhydride was accompanied by heat evolution) in an ice-bath, and the resulting solid was filtrated and dried at room temperature. Ion-exchange was performed with the proportion of 250 mL of iron solution per 3 g of zeolite (stirring under reflux, at 85 °C, for 6 h). The solution concentration was calculated based on the sample theoretical ion-exchange capacity (with molar excess  $\mu = 0.4$ ). In the case of the samples exchanged with  $\text{FeSO}_4 \cdot 7\text{H}_2\text{O}$ , the slurry was kept under Ar atmosphere, in order to avoid iron oxidation. After modification with iron, the resulting samples were quenched in an ice-bath, centrifuged, washed with distilled water, dried at 60 °C, overnight, and finally calcined at 600 °C for 6 h.

## 3.2. Catalysts Characterization

The X-ray diffractograms were obtained with a Bruker D2 Phaser instrument. The patterns were recorded with a step of 0.02° and a counting time of 1 s per step.

The textural parameters were determined by  $\text{N}_2$  adsorption at −196 °C, using a 3Flex v1.00 (Micromeritics, Norcross, GA, USA) automated gas adsorption system. Prior to the analysis, the samples

were outgassed under vacuum at 350 °C for 24 h. BET surface area of the samples was determined according to the recommendations of Rouquerol et al. [52]

The chemical composition of the samples was determined by ICP-OES method, using an iCAP 7400 instrument (Thermo Science, Waltham, MA, USA).

The UV-vis-DRS were recorded by using an Evolution 600 (Thermo, Waltham, MA, USA) spectrophotometer in the range of 200–900 nm, with a resolution of 2 nm.

High-Resolution Transmission Electron Micrographs (HRTEM) were collected by a JEOL JEM2100F (Thermo Science, Waltham, MA, USA) electron microscope, operating at 200 kV.

The H<sub>2</sub>-TPR measurements were carried out from room temperature up to 950 °C, with a linear heating rate of 10 °C/min, using 5 vol.% H<sub>2</sub> diluted in Ar (flow rate 10 mL/min). Before reduction 0.05 g, the sample was outgassed at 500 °C, for 20 min, in Ar flow. The hydrogen uptake was analyzed with the use of a thermal conductivity detector (TCD, VICI-Valco instruments, Houston, TX, USA).

### 3.3. Catalytic Tests

Catalytic studies of N<sub>2</sub>O decomposition were performed in a fixed-bed quartz microreactor, with the use of 0.1 g of catalyst, with particle sizes in the range of 0.160–0.315 mm. A gas mixture containing 1000 ppm of N<sub>2</sub>O and 40,000 ppm of O<sub>2</sub> in He (total flow rate of 50 mL/min) was used, and the outlet gases were analyzed by using a gas chromatograph (SRI 8610C, Torrance, CA, USA) equipped with a TCD detector. Before each catalytic test, the samples were outgassed at 600 °C for 1 h.

## 4. Conclusions

In the presented studies, layered MCM-22-type zeolite was modified in order to achieve the highest activity in N<sub>2</sub>O decomposition. Modification of MCM-22 and ITQ-2 (delaminated zeolite) with FeSO<sub>4</sub>·7H<sub>2</sub>O and [Fe<sub>3</sub>(OCOCH<sub>3</sub>)<sub>7</sub>·OH·2H<sub>2</sub>O]NO<sub>3</sub> oligocations by ion-exchange method revealed the correlation between the iron precursor used and the form iron species deposited into the samples. The ion-exchange method, using Fe<sup>3</sup>(III) oligocations as iron precursor, resulted in larger metal loadings in the form of well-dispersed iron particles, mainly oligomeric Fe<sub>x</sub>O<sub>y</sub> species. In the case of ion-exchange with “conventional” salt of Fe(II), iron was introduced preferably in the form of monomeric cations, possibly located in ion-exchange positions, with the small contribution of more aggregated species. The obtained results are consistent with our previous studies focused on modification of other zeolites, like ZSM-5 and Beta, with iron Fe<sup>3</sup>(III) oligocations [45,53,54]. Higher activity in N<sub>2</sub>O decomposition of the samples prepared by ion-exchange with Fe<sup>3</sup>(III) oligocations (Fe(O,IE)MCM-22 and Fe(O,IE)ITQ-2) was connected to the presence of oligomeric iron species. Although it is a prospective material for the application in catalysis (e.g., see References [2,10,14]), ITQ-2 zeolite, prepared by delamination of MCM-22, was not found to be more active in the presented studies. It could be connected with the partial destruction of the zeolitic structure (decrease in textural parameters characteristic of microporous zeolites), lower content of introduced iron (delamination slightly decreases acidity and ion-exchange properties), and finally with lower aggregation of introduced iron species (generated porosity and more open structure favors better distribution of metal).

Modification of the samples with iron by direct synthesis (series FeX(N,DS)MCM-22) resulted mainly in introduction of isolated Fe<sup>3+</sup>. The catalysts modified by direct synthesis did not show satisfactory activity in N<sub>2</sub>O decomposition, which is consistent with the earlier studies of framework Fe substituted ZSM-5 [26,42].

Subsequent modification of Fe<sub>2</sub>(N,DS)MCM-22 with FeSO<sub>4</sub>·7H<sub>2</sub>O or [Fe<sub>3</sub>(OCOCH<sub>3</sub>)<sub>7</sub>·OH·2H<sub>2</sub>O]NO<sub>3</sub> oligocations by ion-exchange method did not result in any synergetic effects of Fe introduced into the zeolite framework and the other forms of iron introduced by ion-exchange method. Despite the higher iron content and the presence of oligomeric Fe<sub>x</sub>O<sub>y</sub> species (selected in the previous stage of the studies as the most active ones), the catalytic efficiency of the samples did not increase. It seems that the decrease in surface textural parameters caused by agglomeration of iron species introduced by

subsequent modification and zeolite pore blocking was responsible for the lower catalytic activity of the samples in N<sub>2</sub>O decomposition.

Among the examined iron precursors and modification methods, deposition of [Fe<sub>3</sub>(OCOCH<sub>3</sub>)<sub>7</sub>·OH·2H<sub>2</sub>O]NO<sub>3</sub> oligocations by ion-exchange method into MCM-22 was found as the most promising for the activation of MWW zeolites in the reaction of N<sub>2</sub>O decomposition. Ion-exchange method used for deposition of Fe<sup>3</sup>(III) oligocations into zeolites enabled introduction of larger iron content in comparison to ion-exchange with FeSO<sub>4</sub>·7H<sub>2</sub>O solution. Iron introduced by this way was uniformly distributed in the sample and was present mainly in the form of oligomeric species, which were postulated to be the most catalytically active in N<sub>2</sub>O decomposition. This modification method is not limited only to MCM-22 zeolite or N<sub>2</sub>O decomposition and can be very promising for the application in other catalytic systems.

**Author Contributions:** Conceptualization, M.R., U.D., and L.C.; methodology, M.R. and L.C.; investigation, M.R., A.J., E.R.-D., W.D., A.K., Z.P. and S.L.; writing—M.R.; original draft preparation, M.R.; writing—review and editing, U.D. and L.C.; visualization, M.R.; supervision, L.C. All authors have read and agreed to the published version of the manuscript.

**Funding:** This work was carried out in the frame of project No. 0670/IP3/2016/74, from the Polish Ministry of Science and Higher Education, in the years 2016–2019. Part of the work was performed in the frame of project No. 2012/05/B/ST5/00269, from the National Science Centre (Poland). U.D. acknowledges the Spanish Government for funding (MAT2017-82288-C2-1-P).

**Conflicts of Interest:** The authors declare no conflict of interest.

## References

1. Rubin, M.K.; Chu, P. Composition of Synthetic Porous Crystalline Material, Its Synthesis and Use. U.S. Patent No 4954325, 06 November 1990.
2. Osman, M.; Al-Khattaf, S.; Díaz, U.; Martínez, C.; Corma, A. Influencing the activity and selectivity of alkylaromatic catalytic transformations by varying the degree of delamination in MWW zeolites. *Catal. Sci. Technol.* **2016**, *6*, 3166–3181. [\[CrossRef\]](#)
3. Xing, E.; Shi, Y.; Xie, W.; Zhang, F.; Mu, X.; Shu, X. Temperature-controlled phase-transfer hydrothermal synthesis of MWW zeolites and their alkylation performances. *RSC Adv.* **2016**, *6*, 29707–29717. [\[CrossRef\]](#)
4. Gallego, E.M.; Paris, C.; Martínez, C.; Moliner, M.; Corma, A. Nanosized MCM-22 zeolite using simple nonsurfactant organic growth modifiers: Synthesis and catalytic applications. *Chem. Commun.* **2018**, *54*, 9989–9992. [\[CrossRef\]](#) [\[PubMed\]](#)
5. Wang, Y.; Gao, Y.; Xie, S.; Liu, S.; Chen, F.; Xin, W.; Zhu, X.; Li, X.; Jiang, N.; Xu, L. Adjustment of the Al siting in MCM-22 zeolite and its effect on alkylation performance of ethylene with benzene. *Catal. Today* **2018**, *316*, 71–77. [\[CrossRef\]](#)
6. Lim, T.H.; Nam, K.; Song, I.K.; Lee, K.-Y.; Kim, D.H. Effect of Si/Al<sub>2</sub> ratios in Mo/H-MCM-22 on methane dehydroaromatization. *Appl. Catal. A Gen.* **2018**, *552*, 11–20. [\[CrossRef\]](#)
7. Lee, W.; Lee, T.; Jang, H.-G.; Cho, S.J.; Choi, J.; Ha, K.-S. Effects of hierarchical zeolites on aromatization of acetylene. *Catal. Today* **2018**, *303*, 177–184. [\[CrossRef\]](#)
8. Zhang, L.; Wang, H.; Liu, G.; Gao, K.; Wu, J. Methanol-to-olefin conversion over H-MCM-22 catalyst. *J. Mol. Catal. A Chem.* **2016**, *411*, 311–316. [\[CrossRef\]](#)
9. Chen, J.; Liang, T.; Li, J.; Wang, S.; Qin, Z.; Wang, P.; Huang, L.; Fan, W.; Wang, J. Regulation of framework aluminum siting and acid distribution in H-MCM-22 by boron incorporation and its effect on the catalytic performance in methanol to hydrocarbons. *ACS Catal.* **2016**, *6*, 2299–2313. [\[CrossRef\]](#)
10. Carriço, C.S.; Cruz, F.T.; Dos Santos, M.B.; Oliveira, D.S.; Pastore, H.O.; Andrade, H.M.C.; Mascarenhas, A.J.S. MWW-type catalysts for gas phase glycerol dehydration to acrolein. *J. Catal.* **2016**, *334*, 34–41. [\[CrossRef\]](#)
11. Dos Santos, M.B.; Andrade, H.M.C.; Mascarenhas, A.J.S. Oxidative dehydration of glycerol over alternative H,Fe-MCM-22 catalysts: Sustainable production of acrylic acid. *Microporous Mesoporous Mater.* **2019**, *278*, 366–377. [\[CrossRef\]](#)
12. Wang, Y.; Yokoi, T.; Namba, S.; Kondo, J.N.; Tatsumi, T. Improvement of catalytic performance of MCM-22 in the cracking of n-hexane by controlling the acidic property. *J. Catal.* **2016**, *333*, 17–28. [\[CrossRef\]](#)

13. Hussain, A.I.; Aitani, A.M.; Kubů, M.; Čejka, J.; Al-Khattaf, S. Catalytic cracking of Arabian Light VGO over novel zeolites as FCC catalyst additives for maximizing propylene yield. *Fuel* **2016**, *167*, 226–239. [\[CrossRef\]](#)
14. Hao, Q.-Q.; Lei, C.-Y.; Song, Y.-H.; Liu, Z.-T.; Liu, Z.-W. The delaminating and pillaring of MCM-22 for Fischer–Tropsch synthesis over cobalt. *Catal. Today* **2016**, *274*, 109–115. [\[CrossRef\]](#)
15. Wojtaszek-Gurdak, A.; Calvino-Casilda, V.; Grzesinska, A.; Martin-Aranda, R.; Ziolk, M. Impact of Brønsted acid sites in MWW zeolites modified with cesium and amine species on Knoevenagel condensation. *Microporous Mesoporous Mater.* **2019**, *280*, 288–296. [\[CrossRef\]](#)
16. Ma, X.; Zhou, D.; Chu, X.; Li, D.; Wang, J.; Song, W.; Xia, Q. Highly selective isomerization of biomass  $\beta$ -pinene over hierarchically acidic MCM-22 catalyst. *Microporous Mesoporous Mater.* **2017**, *237*, 180–188. [\[CrossRef\]](#)
17. Štekrová, M.; Kubů, M.; Shamzhy, M.; Musilová, Z.; Čejka, J.  $\alpha$ -Pinene oxide isomerization: Role of zeolite structure and acidity in the selective synthesis of campholenic aldehyde. *Catal. Sci. Technol.* **2018**, *8*, 2488–2501. [\[CrossRef\]](#)
18. Rutkowska, M.; Díaz, U.; Palomares, A.E.; Chmielarz, L. Cu and Fe modified derivatives of 2D MWW-type zeolites (MCM-22, ITQ-2 and MCM-36) as new catalysts for DeNO<sub>x</sub> proces. *Appl. Catal. B Environ.* **2015**, *168–169*, 531–539. [\[CrossRef\]](#)
19. Wojtaszek-Gurdak, A.; Sobczak, I.; Grzelak, K.; Ziolk, M.; Hartfelder, U.; Van Bokhoven, J.A. The role of pillaring in MCM-22 on the dispersion of noble metals and catalytic activity. *Mater. Res. Bull.* **2016**, *76*, 169–178. [\[CrossRef\]](#)
20. Roth, W.J.; Kresge, C.T.; Vartuli, J.C.; Leonowicz, M.E.; Fung, A.S.; McCullen, S.B. MCM-36: The first pillared molecular sieve with zeoliteproperties. *Stud. Surf. Sci. Catal.* **1995**, *94*, 301–308.
21. Corma, A.; Fornés, V.; Pergher, S.; Maesen, T.L.M.; Buglass, J.G. Delaminated zeolite precursors as selective acidic catalysts. *Nature* **1998**, *396*, 353–356. [\[CrossRef\]](#)
22. Corma, A.; Fornés, V.; Guil, J.M.; Pergher, S.; Maesen, T.L.M.; Buglass, J.G. Preparation, characterisation and catalytic activity of ITQ-2, a delaminated zeolite. *Microporous Mesoporous Mater.* **2000**, *38*, 301–309. [\[CrossRef\]](#)
23. Corma, A.; Díaz, U.; Fornés, V.; Guil, J.M.; Martínez-Triguero, J.; Creighton, E.J. characterization and catalytic activity of MCM-22 and MCM-56 compared with ITQ-2. *J. Catal.* **2000**, *191*, 218–224. [\[CrossRef\]](#)
24. Kapteijn, F.; Rodriguez-Mirasol, J.; Moulijn, J.A. Heterogeneous catalytic decomposition of nitrous oxide. *Appl. Catal. B Environ.* **1996**, *9*, 25–64. [\[CrossRef\]](#)
25. Pérez-Ramírez, J.; Kapteijn, F.; Schöffel, K.; Moulijn, J.A. Formation and control of N<sub>2</sub>O in nitric acid production: Where do we stand today? *Appl. Catal. B Environ.* **2003**, *44*, 117–151. [\[CrossRef\]](#)
26. Pérez-Ramírez, J.; Kapteijn, F.; Brückner, A. Active site structure sensitivity in N<sub>2</sub>O conversion over FeMFI zeolites. *J. Catal.* **2003**, *218*, 234–238. [\[CrossRef\]](#)
27. Pirngruber, G.D.; Luechinger, M.; Roy, P.K.; Cecchetto, A.; Smirniotis, P. N<sub>2</sub>O decomposition over iron-containing zeolites prepared by different methods: A comparison of the reaction mechanism. *J. Catal.* **2004**, *224*, 429–440. [\[CrossRef\]](#)
28. Jiša, K.; Nováková, J.; Schwarze, M.; Vondrová, A.; Sklenák, S.; Sobalik, Z. Role of the Fe-zeolite structure and iron state in the N<sub>2</sub>O decomposition: Comparison of Fe-FER, Fe-BEA, and Fe-MFI catalysts. *J. Catal.* **2009**, *262*, 27–34. [\[CrossRef\]](#)
29. Sádovská, G.; Bernauer, M.; Bernauer, B.; Tabor, E.; Vondrová, A.; Sobalik, Z. On the mechanism of high-temperature N<sub>2</sub>O decomposition over Fe-FER in the presence of NO. *Catal. Commun.* **2018**, *112*, 58–62. [\[CrossRef\]](#)
30. Stelmachowski, P.; Maniak, G.; Kotarba, A.; Sojka, Z. Strong electronic promotion of Co<sub>3</sub>O<sub>4</sub> towards N<sub>2</sub>O decomposition by surface alkali dopants. *Catal. Commun.* **2009**, *10*, 1062–1065. [\[CrossRef\]](#)
31. Maniak, G.; Stelmachowski, P.; Stanek, J.J.; Kotarba, A.; Sojka, Z. Catalytic properties in N<sub>2</sub>O decomposition of mixed cobalt–iron spinels. *Catal. Commun.* **2011**, *15*, 127–131. [\[CrossRef\]](#)
32. Abu-Zied, B.M.; Soliman, S.A.; Abdellah, S.E. Enhanced direct N<sub>2</sub>O decomposition over Cu<sub>x</sub>Co<sub>1-x</sub>Co<sub>2</sub>O<sub>4</sub> (0.0  $\leq x \leq 1.0$ ) spinel-oxide catalysts. *J. Ind. Eng. Chem.* **2015**, *21*, 814–821. [\[CrossRef\]](#)
33. Wójcik, S.; Thersleff, T.; Gębska, K.; Grzybek, G.; Kotarba, A. Atomic-Level Dispersion of Bismuth over Co<sub>3</sub>O<sub>4</sub> Nanocrystals—Outstanding Promotional Effect in Catalytic DeN<sub>2</sub>O. *Catalysts* **2020**, *10*, 351. [\[CrossRef\]](#)

34. Wójcik, S.; Grzybek, G.; Stelmachowski, P.; Sojka, Z.; Kotarba, A. Bulk, Surface and Interface Promotion of  $\text{Co}_3\text{O}_4$  for the Low-Temperature  $\text{N}_2\text{O}$  Decomposition Catalysis. *Catalysts* **2019**, *10*, 41. [\[CrossRef\]](#)
35. Pacultová, K.; Karásková, K.; Kovanda, F.; Jiráťová, K.; Šrámek, J.; Kustrowski, P.; Kotarba, A.; Chromčáková, Z.; Kočí, K.; Obalová, L. K-Doped Co-Mn-Al Mixed Oxide Catalyst for  $\text{N}_2\text{O}$  Abatement from Nitric Acid Plant Waste Gases: Pilot Plant Studies. *Ind. Eng. Chem. Res.* **2016**, *55*, 7076–7084. [\[CrossRef\]](#)
36. Pérez-Ramírez, J.; Kapteijn, F.; Moulijn, J.A. High activity and stability of the Rh-free Co-based ex-hydrotalcite containing Pd in the catalytic decomposition of  $\text{N}_2\text{O}$ . *Catal. Lett.* **1999**, *60*, 133–138. [\[CrossRef\]](#)
37. Kovanda, F.; Rojka, T.; Dobešová, J.; Machovič, V.; Bezdičák, P.; Obalová, L.; Jiráťová, K.; Grygar, T. Mixed oxides obtained from Co and Mn containing layered double hydroxides: Preparation, characterization, and catalytic properties. *J. Solid State Chem.* **2006**, *179*, 812–823. [\[CrossRef\]](#)
38. Obalová, L.; Karásková, K.; Jiráťová, K.; Kovanda, F. Effect of potassium in calcined Co–Mn–Al layered double hydroxide on the catalytic decomposition of  $\text{N}_2\text{O}$ . *Appl. Catal. B Environ.* **2009**, *90*, 132–140. [\[CrossRef\]](#)
39. Richards, N.; Nowicka, E.; Carter, J.H.; Morgan, D.J.; Dummer, N.F.; Golunski, S.; Hutchings, G.J. Investigating the Influence of Fe Speciation on  $\text{N}_2\text{O}$  Decomposition Over Fe-ZSM-5 Catalysts. *Top. Catal.* **2018**, *61*, 1983–1992. [\[CrossRef\]](#)
40. Dubkov, K.A.; Ovanesyan, N.S.; Shteinman, A.A.; Starokon, E.V.; Panov, G.I. Evolution of Iron States and Formation of  $\alpha$ -Sites upon Activation of FeZSM-5 Zeolites. *J. Catal.* **2002**, *207*, 341–352. [\[CrossRef\]](#)
41. Pirngruber, G.D. The surface chemistry of  $\text{N}_2\text{O}$  decomposition on iron containing zeolites (I). *J. Catal.* **2003**, *219*, 456–463. [\[CrossRef\]](#)
42. Pérez-Ramírez, J.; Kapteijn, F.; Groen, J.C.; Doménech, A.; Mul, G.; Moulijn, J.A. Steam-activated FeMFI zeolites. Evolution of iron species and activity in direct  $\text{N}_2\text{O}$  decomposition. *J. Catal.* **2003**, *214*, 33–45. [\[CrossRef\]](#)
43. Roth, W.J.; Douglas, L.D. Expanded view of zeolite structures and their variability based on layered nature of 3-D frameworks. *Microporous Mesoporous Mater.* **2011**, *142*, 32–36. [\[CrossRef\]](#)
44. Roth, W.J.; Douglas, L.D.; Kennedy, G.J. Discovery of new MWW family zeolite EMM-10: Identification of EMM-10P as the missing MWW precursor with disordered layers. *Microporous Mesoporous Mater.* **2011**, *142*, 168–177. [\[CrossRef\]](#)
45. Rutkowska, M.; Borcuch, A.; Marzec, A.; Kowalczyk, A.; Samojeden, B.; Moreno, J.M.; Díaz, U.; Chmielarz, L. Influence of iron aggregation on the catalytic performance of desilicated MFI in the  $\text{DeNO}_x$  proces. *Microporous Mesoporous Mater.* **2020**, *304*, 109114–109122. [\[CrossRef\]](#)
46. Pan, H.; Guo, Y.; Bi, H.T.  $\text{NO}_x$  adsorption and reduction with  $\text{C}_3\text{H}_6$  over Fe/zeolite catalysts: Effect of catalyst suport. *Chem. Eng. J.* **2015**, *280*, 66–73. [\[CrossRef\]](#)
47. Romero-Sáez, M.; Divakar, D.; Aranzabal, A.; González-Velasco, J.R.; González-Marcos, J.A. Catalytic oxidation of trichloroethylene over Fe-ZSM-5: Influence of the preparation method on the iron species and the catalytic activity. *Appl. Catal. B Environ.* **2016**, *180*, 210–218. [\[CrossRef\]](#)
48. Gao, Y.; Zheng, B.; Wu, G.; Ma, F.; Liu, C. Effect of the Si/Al ratio on the performance of hierarchical ZSM-5 zeolites for methanol aromatization. *RSC Adv.* **2016**, *6*, 83581–83588. [\[CrossRef\]](#)
49. Testa, F.; Crea, F.; Diodati, G.D.; Pasqua, L.; Aiello, R.; Terwagne, G.; Lentz, P.; Nagy, J.B. Synthesis and characterization of Fe- and [Fe,Al]-MCM-22 zeolites. *Microporous Mesoporous Mater.* **1999**, *30*, 187–197. [\[CrossRef\]](#)
50. Macina, D.; Piwowarska, Z.; Góra-Marek, K.; Tarach, K.; Rutkowska, M.; Girman, V.; Błachowski, A.; Chmielarz, L. SBA-15 loaded with iron by various methods as catalyst for  $\text{DeNO}_x$  proces. *Mater. Res. Bull.* **2016**, *78*, 72–82. [\[CrossRef\]](#)
51. Macina, D.; Opiola, A.; Rutkowska, M.; Basąg, S.; Piwowarska, Z.; Michalik, M.; Chmielarz, L. Mesoporous silica materials modified with aggregated transition metal species (Cr, Fe and Cr-Fe) in the role of catalysts for selective catalytic oxidation of ammonia to dinitrogen. *Mater. Chem. Phys.* **2017**, *187*, 60–71. [\[CrossRef\]](#)
52. Rouquerol, J.; Llewellyn, P.; Rouquerol, F. Is the BET equation applicable to microporous adsorbents? *Stud. Surf. Sci. Catal.* **2007**, *160*, 49–56.

53. Rutkowska, M.; Duda, M.; Macina, D.; Górecka, S.; Dębek, R.; Moreno, J.M.; Díaz, U.; Chmielarz, L. Mesoporous Beta zeolite functionalisation with  $\text{Fe}_x\text{Cr}_y$  oligocations; catalytic activity in the  $\text{NH}_3$ -SCO proces. *Microporous Mesoporous Mater.* **2019**, *278*, 1–13. [[CrossRef](#)]
54. Borcuch, A.; Rutkowska, M.; Marzec, A.; Kowalczyk, A.; Michalik, M.; Moreno, J.M.; Díaz, U.; Chmielarz, L. Selective ammonia oxidation over ZSM-5 zeolite: Impact of catalyst's suport and type of deposited iron species. *Catal. Today* **2020**, *348*, 223–229. [[CrossRef](#)]



© 2020 by the authors. Licensee MDPI, Basel, Switzerland. This article is an open access article distributed under the terms and conditions of the Creative Commons Attribution (CC BY) license (<http://creativecommons.org/licenses/by/4.0/>).